Article

Application of Back-Propagation Neural Network in the Post-Blast Re-Entry Time Prediction

Jinrui Zhang [1], Chuanqi Li [2,*] and Tingting Zhang [2]

[1] School of Resources & Civil Engineering, Northeastern University, Shenyang 110819, China
[2] Laboratory 3SR, CNRS UMR 5521, Grenoble Alpes University, 38000 Grenoble, France
* Correspondence: chuanqi.li@univ-grenoble-alpes.fr

Abstract: Predicting the post-blast re-entry time precisely can improve productivity and reduce accidents significantly. The empirical formulas for the time prediction are practical to implement, but lack accuracy. In this study, a novel method based on the back-propagation neural network (BPNN) was proposed to tackle the drawbacks. A numerical model was constructed and 300 points of sample data were recorded, with consideration to fresh air volume, occupational exposure limit, toxic gas volume per kg of explosives and roadway length. The BPNN model with six neurons in a hidden layer was then developed and prediction performance was discussed in terms of four indicators, namely, the root mean square error (RMSE), the coefficient of determination (R^2), the mean absolute error (MAE) and the sum of squares error (SSE). Furthermore, one representative empirical formula was introduced and calibrated for the comparison. The obtained results showed that the BPNN model had a more remarkable performance, with RMSE of 21.45 (R^2: 0.99, MAE: 10.78 and SSE: 40934), compared to the empirical formula, with RMSE of 76.89 (R^2: 0.90, MAE: 42.06 and SSE: 526147). Hence, the BPNN model is a superior method for predicting the post-blast re-entry time. For better practical application, it was then embedded into the software.

Keywords: post-blast re-entry time; back-propagation neural network; underground mine

1. Introduction

The number of underground mines is increasing due to the depletion of resources on the surface. The drill and blast (D&B) and tunnel boring machines (TBM) have been used in underground mines for excavation. Although TBM has been adopted at sites such as San Manual Mine and Stillwater Mine [1], many difficulties, including cutter wear and rock popping, etc., have hindered its development [2]. Consequently, D&B is still the main excavation method due to its flexibility and economy [3,4]. However, one of the shortcomings of D&B is that it emits a substantial amount of toxic gases, including carbon monoxide (CO), nitric oxide (NO) and nitrogen dioxide (NO_2). Among them, CO is the primary research object, due to its stability and large quantity [5]. For the purposes of improving cleaning efficiency and enhancing the production capacity, ventilation has been identified as one of the most effective methods and has been used widely [6].

The ventilation time taken to reduce the toxic gas concentration below the occupational exposure limit is defined as the post-blast re-entry time [5]. Additionally, a report has shown that most mines have more than four blasts per day, so estimating the post-blast re-entry time as accurately as possible will avoid the loss of significant amounts of production time [7]. Several methods have been studied and applied. For example, many mines have relied on the fixed-time interval to determine when the miners can re-enter the heading face to work continuously [8]. However, it should be noted that this may lead to a number of associated safety and health issues for workers. In order to improve accuracy, some empirical formulas were developed by using the flow balance, fitting the data obtained from numerical simulations, site tests, and laboratory experiments [4,7,9–15]. Despite

the considerable advantages of empirical formulas, such as being simple, convenient, and timesaving, the calculation is less universal so that some parameters such as the dilution efficiency factor, need to be calibrated according to the particular mine where the concentration data can be monitored [15].

As opposed to the empirical formulas, artificial intelligence (AI) technologies have a good history of performance in prediction [16]. The technique has gained popularity in many fields, including UCS of rock [17,18], shear strength of rockfill material [19], backbreak in open-pit mines [20], ozone concentration [21] and carbon monoxide concentration [22]. Additionally, the AI technologies have the ability to consider several factors, and the results can be obtained directly based on the optimized AI model. AI can also avoid the above-mentioned limitations of the empirical formula. However, AI technologies have rarely been implemented into the re-entry time prediction, to the author's knowledge.

Gathering reliable sample data is necessary for the construction of AI models [23]. Field data is of course the most reliable type, but one that is not easy to access, due to the harsh environment in the mines [24]. On the contrary side, numerical simulation has gained worldwide attention in the study of the migration behaviors of blasting production in the underground roadway, owing to the superiority of visualization, data richness and ease of operation [25–28]. However, the length of these models is typically short, as numerical simulation requires a high level of computational performance, especially for long roadways with a significant amount of nodes. The Ventsim software, which is based on the Hardy Cross algorithm, and which has been used to study the post-blast re-entry time in some complex roadways with affordable computation time [15,29], was thus selected to calculate the time under various conditions in this study.

Therefore, this paper aims to develop a BPNN model for predicting the post-blast re-entry time. The rest of this study is organized as follows. The section titled "Model process and data preparation" introduces the construction of models used, as well as the process of database establishment, including the selection and analysis of parameter ranges. The section titled "Methodology" describes the algorithm of BPNN as well as the process of calibrating the empirical formula in detail, in addition to four indicators adopted to evaluate the performance of proposed models. The section titled "Results and discussions" contains the description of building the architecture of the BPNN and a performance comparison of both models for the time prediction. The section titled "Algorithm embedding" exhibits one software developed based on the proposed models. In the last section, the main conclusions and future development are given.

2. Model Process and Data Preparation

2.1. Model Construction

The research object is one cross-section of the roadway at a depth of approximately 580 m below the surface. The section's size and its corresponding 3-D model constructed in Ventsim are shown in Figure 1. It is a three-core arch structure with an area of 14.04 m^2. The width, wall height and arch height are 3.95 m, 2.8 m and 0.95 m, respectively. Facilities such as cables and supports inside the roadway were not taken into consideration. The amount of explosives used each time are about 40 kg and the temperature is around 300 K. It is worth pointing out that the ventilation duct was placed off the roadway in this software for the convenience of real-time viewing of ventilation performance.
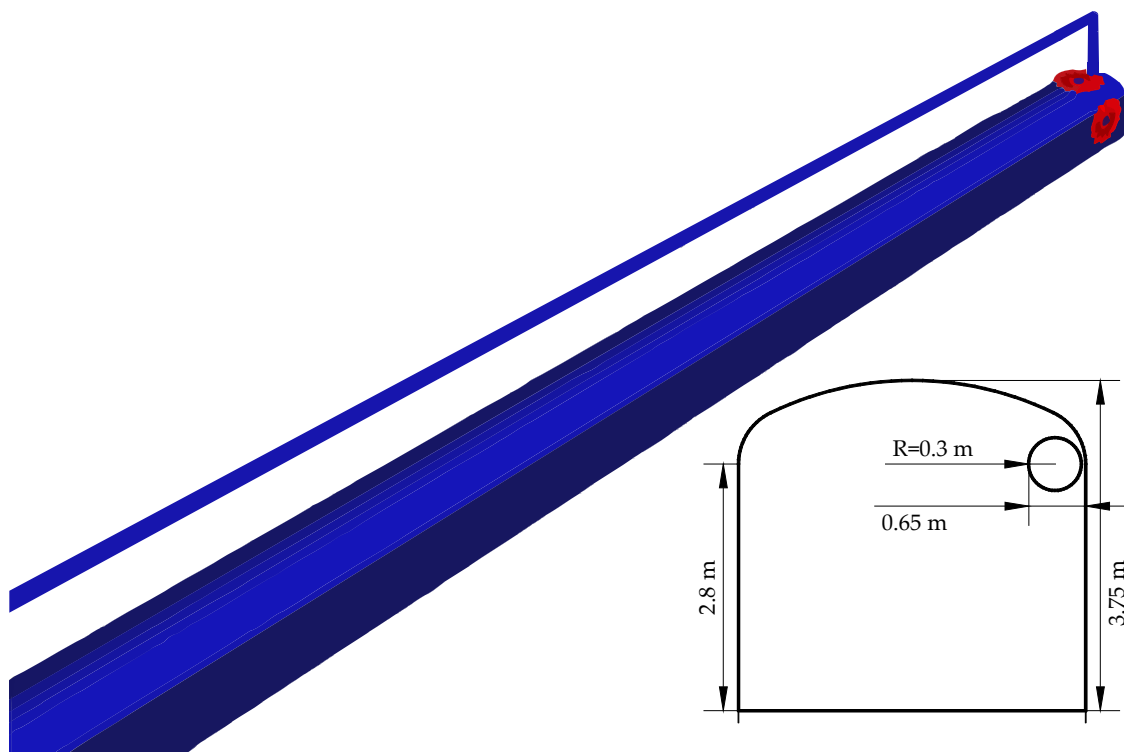
Figure 1. Geometry of researched model.

2.2. Database Generation

Four parameters, namely, average velocity within the roadway, occupational exposure limit, toxic gas volume per kg of explosives and length of roadway, have frequently been considered when calculating the relevant time [11,15]. Hence, these four parameters were also used for developing the BPNN model in this study. Due to the fact that the fresh-air volume of the ventilation duct has a considerable impact on the average velocity within the roadway, the minimal average velocity in the excavation roadway was set at 0.25 m/s and the highest average velocity was set at 4 m/s in the mining area, given in the safety regulations for metal and nonmetal mines of China [30]. As a consequence, the average velocity ranged from 0.25 m/s to 4 m/s in this study. Moreover, some indexes for assessing occupational exposure limit have been proposed, depending upon the actual requirements. For example, time weight average (TWA) is defined as the average permissible concentration within a normal 8 h workday and 40 h work-week. Short term exposure limit (STEL) considers the permissible concentration limit for up to 15 min with the serious implementation of the TWA. Table 1 shows the TWA and STEL of different countries for CO. It can be seen that China has the strictest regulations for exposure concentration, so 24 ppm was used as the monitoring standard rather than the 16 ppm level found in some regulations [31]. Taking all of the above factors into account, the occupational exposure limits in this study were taken to be between 24 ppm and 50 ppm, in order to meet a variety of requirements.

Toxic gas production is susceptible to a variety of influencing factors, such as the sort of explosives [32], the environment of the roadway [33], the type of blasting design, the method of detonation, and so on [34]. Therefore, the amount of toxic gases produced in each detonation varies slightly. The #2 rock emulsion explosive was adopted in this study. The toxic gas volume per kg of explosives in the underground roadway is from 36 L/kg to 42 L/kg, as given by Wang [35]. In addition, the length of the roadway is increased with the continuous construction of excavation engineering. Herein, the range from 200 m up to 1500 m was studied. Figure 2 presents the minimum, lower quartile, median, upper

quartile and maximum for each parameter in boxplots. It illustrates that each parameter shows a uniform distribution.

Table 1. Occupational exposure limit for CO in different countries [13].

	TWA/ppm	STEL/ppm
ASM-2	50	100
NIOSH REL	35	200
NOHSC	30	200
OSHA PEL	35	200
CHINA	16	24

Note: ASM-2 is Instructions Technique Complementary to Mining Safety Actions (Spain); NIOSH is the National Institute for Occupational Safety and Health; NOHSC is the National Occupational Health and Safety Commission; OSHA is the Occupational Safety and Health Administration.
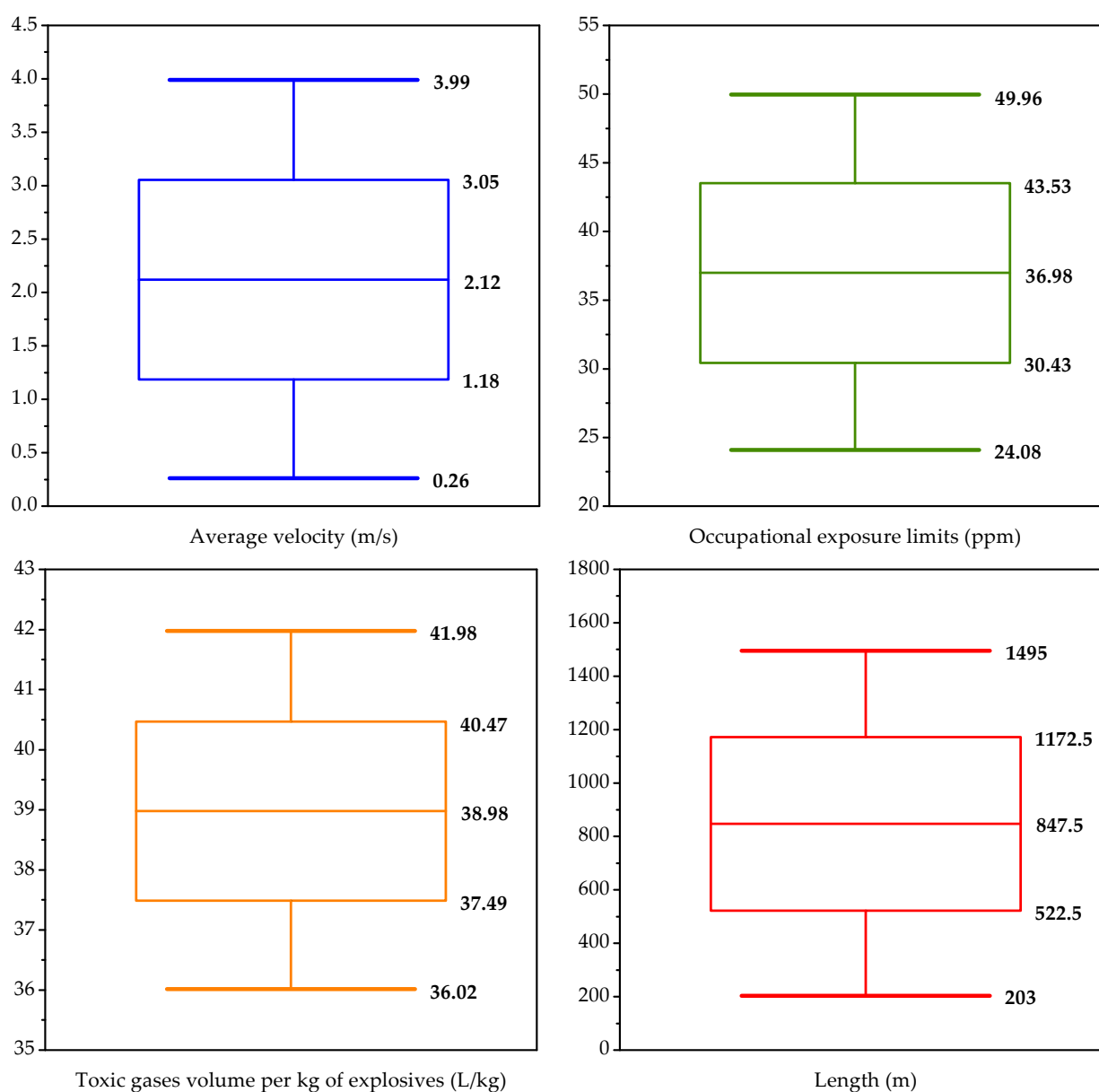

Figure 2. Boxplots of input parameters.

A total of 300 input samples were generated based on the ranges mentioned above, and then these models with specific parameter values were constructed and simulated in Ventsim software to predict the post-blast re-entry time. In total, 300 pieces of data were archived herein as described in Appendix A. The correlation matrix of the dataset is presented in Figure 3. The distributions and correlation coefficients for any two parameters are presented in the lower and upper of this figure, respectively. For the lower, it is clear that the relationship between the inputs and outputs is nonlinear where only the relationship of velocity versus time reveals a distribution similar to a negative exponential. For the upper, the darker the blue, the stronger the negative correlation. Conversely, the lighter the red, the weaker the positive correlation. As can be observed, the correlation coefficient between the four input parameters is low, as they are independent of each other. Additionally, both length and velocity show statistically significant relationships with the time, after significance tests. Despite the fact that gas and limit have lower correlation coefficients, these parameters still remain valid for the subsequent comparative analysis with the empirical formula.
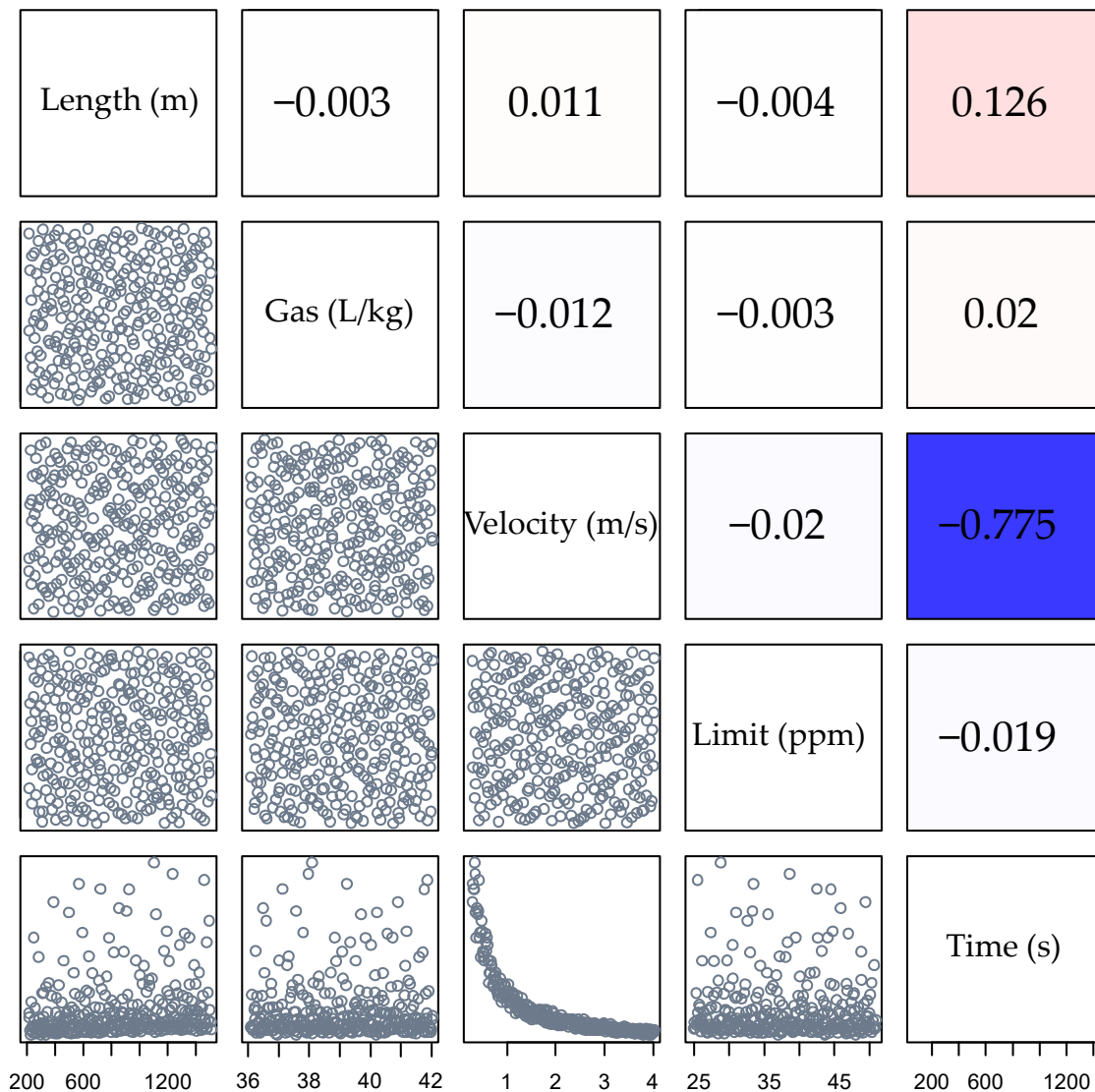

Figure 3. Correlation between input and output parameters.

3. Methodology

3.1. BPNN Algorithm

BPNN is a classical supervised learning method fusing the feedforward neural network and the back-propagation algorithm. It has been used in many fields and achieved excellent performance because of its capabilities of outstanding nonlinear fitting and generalization. For instance, Li et al. [23] have successfully used a BPNN model to predict the stress values when evaluating pillar stability. Zhao et al. [36] applied an integrated model based on the traditional BPNN to predict air pollution concentration and demonstrated that the method is more practical. Hence, BPNN was chosen in this study for predicting the post-blast re-entry time. There are five steps, namely, initialization of weights and biases, feedforward propagation of data, back-propagation of error, optimization of weights and biases and judgment of termination conditions.

At first, weights w and biases θ at the hidden layer and output layer are initialized with random numbers. The magnitude of each weight stands for the degree of influence of the connected neurons on the output, while the bias represents the level of difficulty in generating activation. After that, the accumulation of y_j in the hidden layer and z_k in the output layer can be calculated by the following formulas, respectively:

$$y_j = f\left(\sum_{i=1}^{n}\left(w_{ij} \times x_i\right) - \theta_j\right) (i = 1, 2, \cdots n\,; j = 1, 2, \cdots m) \tag{1}$$

$$z_k = f\left(\sum_{j=1}^{m}\left(w_{jk} \times y_j\right) - \theta_k\right) (j = 1, 2, \cdots m\,; k = 1, 2, \cdots l) \tag{2}$$

where f is an activation function; x, y and z are the output values of the input layer, hidden layer and output layer, respectively; and n, m and l represent the number of neurons at the input layer, hidden layer and output layer, respectively.

Afterward, the back-propagation is performed. The neuron error in the hidden layer and the output layer are E_j and E_k, respectively. As the error is the functions of weights, the tuning weights Δw_{ij} between the input layer and the hidden layer as well as the tuning weights Δw_{jk} between the hidden layer and the output layer are as follows:

$$\Delta w_{ij} = -\eta \frac{\partial E_j}{\partial w_{ij}} \tag{3}$$

$$\Delta w_{jk} = -\eta \frac{\partial E_k}{\partial w_{jk}} \tag{4}$$

where η is the learning rate.

Subsequently, the updated weights w_{ij} ($t + 1$) and w_{jk} ($t + 1$) are given as:

$$w_{ij}(t+1) = w_{ij}(t) + \Delta w_{ij} \tag{5}$$

$$w_{jk}(t+1) = w_{jk}(t) + \Delta w_{jk} \tag{6}$$

where t represents the number of iterations.

Finally, the process of training is conducted until the convergence conditions are satisfied, or otherwise, these steps (except for the initialization) are looped. In total, the framework of this research based on the BPNN model can be found in Figure 4.
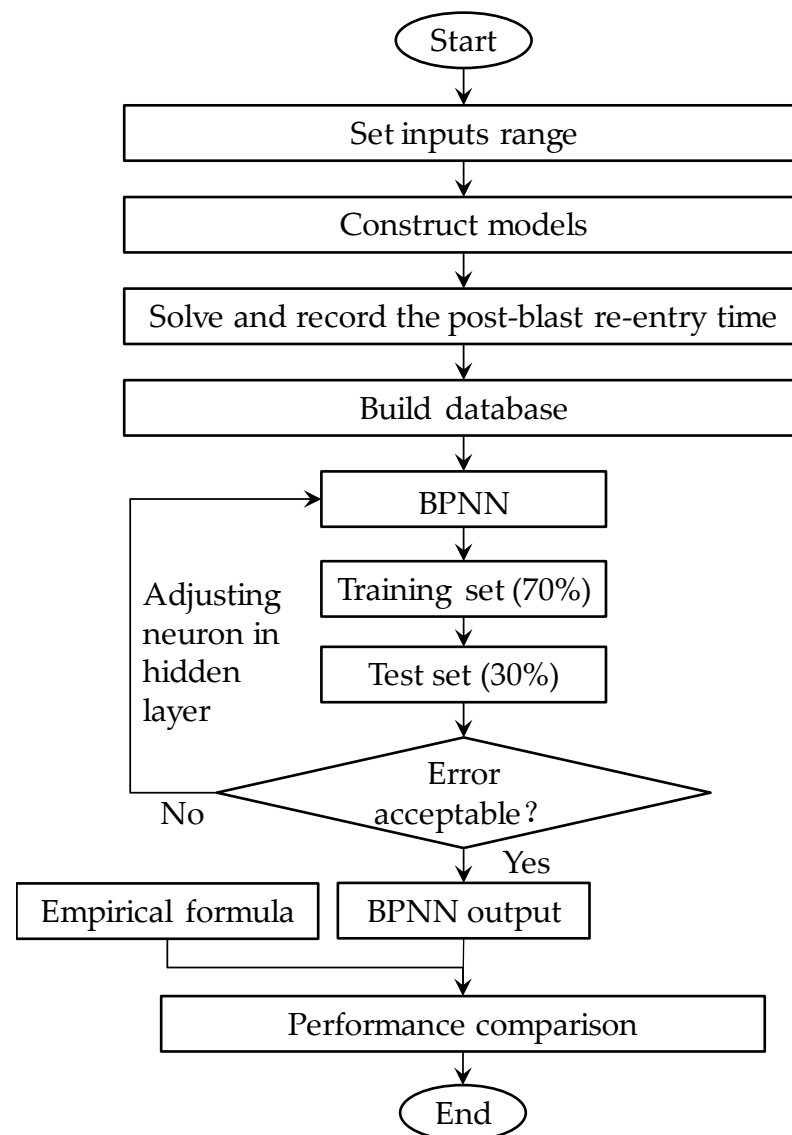
Figure 4. Flowchart of the research process.

3.2. Calibrating Empirical Formula

The schematic of ventilation in the longitudinal profile of the roadway is presented in Figure 5. It is given that the length of the working area and roadway are L_0 and L, respectively. The area of roadway is S. The fresh air volume discharged from the ventilation duct is Q and the toxic gases concentration uniformly distributed in the working area of volume V is C_0 at the initial moment. According to the flow balance, the amount of toxic gases removed after Δt time of ventilation is $Q \times \Delta t$. Hence, the concentration C after T time of ventilation can be calculated by the following:

$$C = \lim_{n \to \propto} C_0 \left(\frac{V - Q\Delta t}{V}\right)^n = \lim_{\Delta t \to 0} C_0 \left(1 - \frac{Q\Delta t}{V}\right)^{\frac{T}{\Delta t}} = C_0 e^{-\frac{TQ}{V}} \tag{7}$$

where n is the ratio of T to Δt.
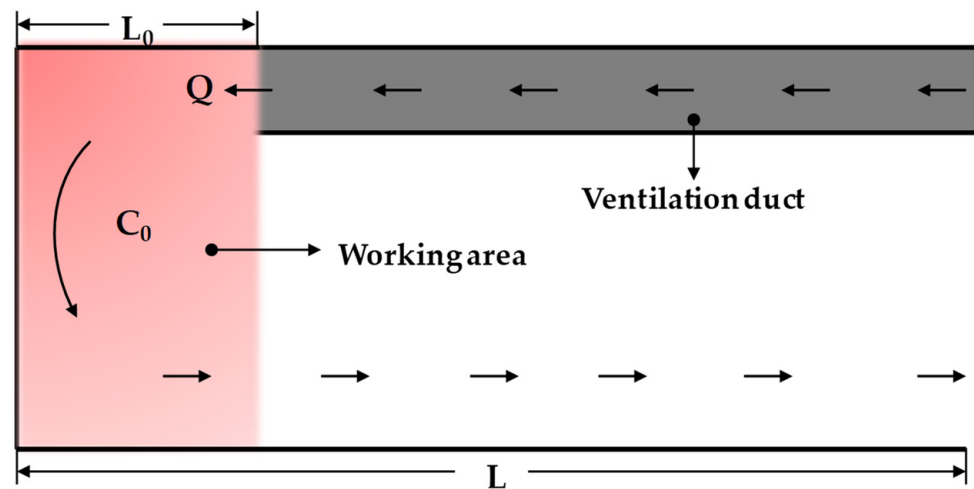
Figure 5. Schematic of ventilation.

Moreover, Equation (7) can be further written by taking the logarithm as:

$$T = \frac{V}{Q} \ln \frac{C_0}{C} \tag{8}$$

Furthermore, some other empirical formulas shown in Table 2 have been developed by using different techniques such as mathematical derivation, data fitting and formula calibration. Among them, the empirical formula given by [15] was selected for comparison with the BPNN model because it provides some optimization based on Equation (8) and is more representative than others.

To acquire dilution efficiency factor f_d in the formula given by [15], the sample with the post-blast re-entry time of 86 s, velocity of 3.79 m/s, length of 474 m, gas production of 36.2 L/kg and exposure limit value of 34 ppm was randomly picked. Some other parameters, namely the working space Vw, fresh air quantity Q and gas concentration C need to be calculated as follows, respectively:

$$V_w = \frac{G \times b}{x_0} \tag{9}$$

$$Q = u \times A \tag{10}$$

$$C = \frac{28 \times G \times b}{29 \times l \times A - G \times b} \tag{11}$$

$$l = 15 + \frac{G}{5} \tag{12}$$

where G is the mass of the explosive, kg; b is the toxic gas volume per kg of explosives, m^3/kg; x_0 is the peak concentration of gas at the entrance monitored, ppm; and l is the throwing distance of toxic gas, m.

Table 2. Empirical formulas for time prediction.

Reference	Equation	Way
[4]	$C = \dfrac{V_G}{2A\sqrt{\pi DT}} e^{\left(\frac{-(L-uT)^2}{4DT}\right)}$	Calibration
[7]	$T = e^{-\left(\frac{Q-60.119}{12.924}\right)}$	Calibration
[7]	$T = 2383.7Q^{-1.574}$	Calibration
[9]	$C = p_1 T_n + p_2 T_{n-1} + \cdots + p_n T + p_{n+1}$	Fitting
[9]	$C = 1048 e^{-\left(\frac{T-6.464}{0.8676}\right)^2}$	Fitting
[10]	$T = 13.118 e^{0.0017L}$	Fitting
[11]	$T = n \ln\left(\dfrac{C}{C_T}\right)$	Derivation
[11]	$T = \dfrac{V}{Q+Q_g} \ln\left[\dfrac{(Q_g+QB_g)-(Q+Q_g)C}{(Q_g+QB_g)-(Q+Q_g)C_T}\right]$	Derivation
[15]	$T = \dfrac{V_w}{Q \times f_d} \ln\left(\dfrac{C}{C_T}\right)$	Calibration

Note: T: ventilation time required, min or s; Q: fresh air quantity, m^3/s; C: gas concentration at the beginning of ventilation, ppm; $p_1, p_2, \ldots, p_{n+1}$: fitting constants; V_W: volume of working space, m^3; f_d: dilution efficiency factor; C_T: gas concentration at time T, ppm; V_G: volume of gas at the heading and beginning of time, m^3; A: area of cross-section of roadway, m^2; D: effective axial dispersion factor, m^2/s; L: distance away from the heading, m; u: average air velocity, m/s; n: numbers of fresh air which is passing through the working space; Q_g: inflow rate of the toxic gases, m^3/s; and B_g: concentration of toxic gases in the ventilation duct, %.

After that, the dilution efficiency factor of 0.73 can be obtained. The final empirical formula, which was employed to calculate the post-blast re-entry time and then compared to the BPNN, is given below:

$$T = \frac{V_w}{0.73Q} \ln\left(\frac{C}{C_T}\right) \tag{13}$$

3.3. Performance Indicators for the Assessment of Models

Four performance indicators, the root mean square error (RMSE), the coefficient of determination (R^2), the mean absolute error (MAE) and the sum of squares error (SSE) were chosen to evaluate the performance of the models developed in this study [37]. Among them, RMSE is taken to measure the deviation between the actual value and the predicted value, where the smaller the value, the better the model's performance. R^2 is available to represent the goodness of fit of the model to the sample data. The closer it is to 1, the stronger the fit is. MAE can reflect the extent of actual prediction error, with smaller values indicating that the prediction is closer to the actual value. SSE is the accumulation of squared error between the predicted value and the actual value. A larger value means a worse quality model when the number of samples is the same. They are defined by the following:

$$\text{RMSE} = \sqrt{\frac{1}{n}\sum_{i=1}^{n}\left(Time_{o,i} - Time_{p,i}\right)^2} \tag{14}$$

$$\text{R}^2 = 1 - \frac{\sum_{i=1}^{n}\left(Time_{o,i} - Time_{p,i}\right)^2}{\sum_{i=1}^{n}\left(Time_{o,i} - \overline{Time_o}\right)^2} \tag{15}$$

$$\text{MAE} = \frac{1}{n}\sum_{i=1}^{n}\left| Time_{o,i} - Time_{p,i}\right| \tag{16}$$

$$\text{SSE} = \sum_{i=1}^{n}\left(Time_{o,i} - Time_{p,i}\right)^2 \tag{17}$$

where n is the number of samples; $Time_{o,i}$, $Time_{p,i}$ are the post-blast re-entry time of actual value and the predicted value, respectively; and $\overline{Time_o}$ represents the mean value of actual post-blast re-entry time.

4. Results and Discussion

4.1. Building the Architecture of the BPNN

An excellent BPNN model, one which has the best weights obtained from the training phase, can predict the post-blast re-entry time precisely. In this study, the BPNN model built on MATLAB was trained and tested with 210 samples (70%) and 90 samples (30%), respectively. The changes in RMSE and R^2 were recorded while the model had a different number of neurons at the hidden layer, as shown in Table 3. It can be summarized that the model with six neurons in the hidden layer performed best in which the lowest RMSE of 12.6171 and the highest R^2 of 0.9975 can be acquired. At the same time, it also has a remarkable performance in the testing phase. Hence, this model was served as the final post-blast re-entry time prediction model and the schematic diagram is presented in Figure 6.

Table 3. Performance of BPNN models with different numbers of neurons in the hidden layer.

Model	Neurons	RMSE		R^2	
		Training	Testing	Training	Testing
1	2	16.0196	21.9249	0.9959	0.9922
2	3	55.9012	37.0202	0.9502	0.9776
3	4	72.4646	60.601	0.9163	0.9401
4	5	61.6996	50.5617	0.9393	0.9583
5	6	12.6171	21.3421	0.9975	0.9926
6	7	14.3551	21.026	0.9967	0.9928
7	8	14.7677	21.4577	0.9965	0.9925
8	9	14.2703	22.0516	0.9968	0.9921
9	10	13.1419	21.6439	0.9973	0.9924

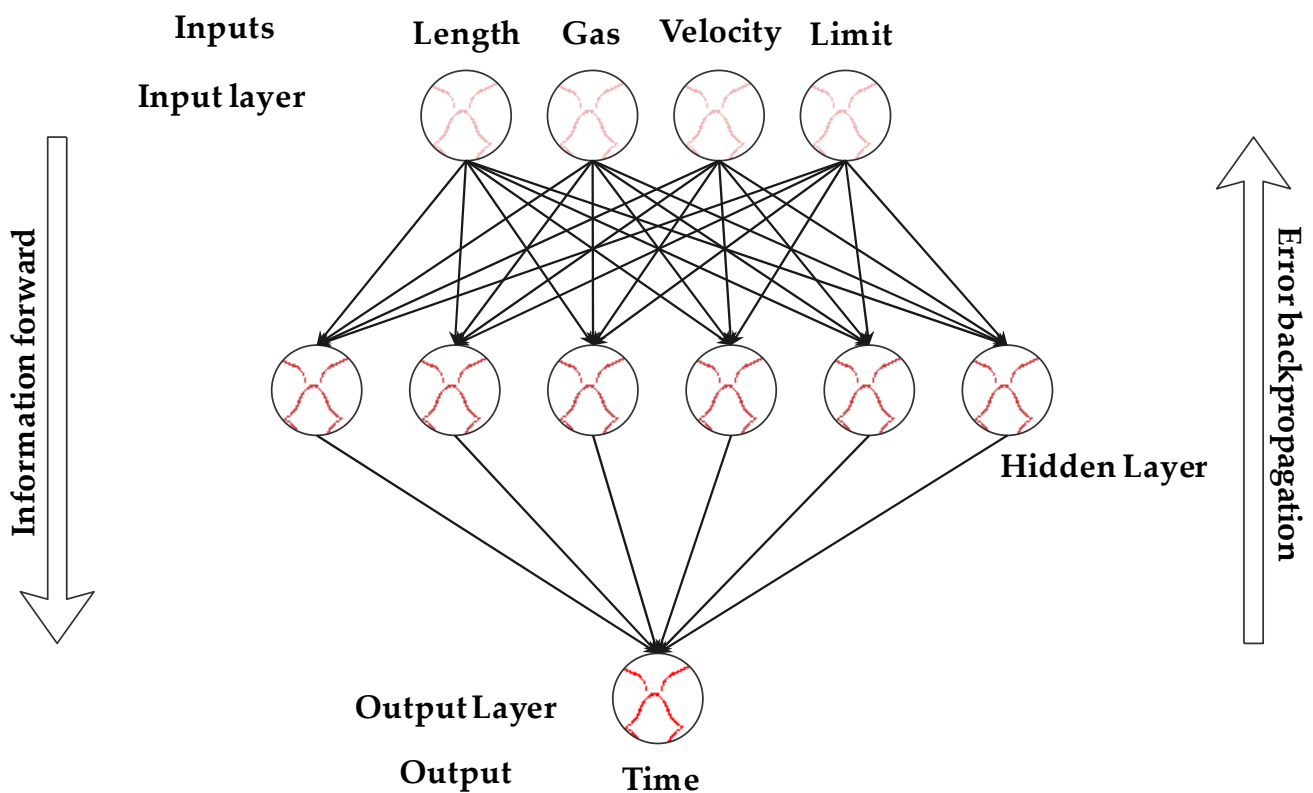Note: the line in bold type indicates the best model.

Figure 6. Proposed BPNN model for predicting time.

4.2. Performance Comparison between BPNN and Formula

The BPNN and empirical formula previously developed were run to predict the post-blast re-entry time in the training set and the test set. The models' performance, including RMSE, R^2, MAE and SSE, was summarized in Table 4. As can be seen in this table, the BPNN model has a better performance in both the training set and the test set than does the empirical formula. The average prediction error of BPNN in the test set is only 10.78 s, which is approximately a quarter of the empirical formula. Additionally, the goodness of fit of BPNN is closer to 1, indicating that it can better account for the relationship between the inputs and output than can the empirical formula. It should be noted that the delay caused by the empirical formula each time will accumulate with the increasing number of detonations. To reduce the losses, the BPNN model should be adapted to predict the post-blast re-entry time.

Table 4. Performance comparison of both models.

Indicators	Training		Testing	
	Empirical	BPNN	Empirical	BPNN
RMSE	61.81	12.61	76.89	21.34
MAE	38.34	7.66	42.06	10.78
R^2	0.94	0.99	0.90	0.99
SSE	798352	33429	526147	40934

In order to compare the performance of both models more exactly, the regression diagrams in the training phase and the testing phase are described in Figure 7. The horizontal axes represent the actual time. The vertical axes render the prediction value obtained from the BPNN and the empirical formula. The slope of diagonal lines with the black color is 1. Other radical lines with deviations of 10% and 30% from the diagonal lines are also drawn in this diagram. Taken as a whole, the BPNN model has a higher accuracy than does the empirical formula in both sets, because the data points are closer to the diagonal line, whereas some data points obtained from the empirical formula are far outside of the line of 30%, especially in the testing phase. It can also be seen that most of them are larger than the actual time when the ventilation time required is larger than 400 s. At the same time, the BPNN in the testing phase has a larger error than in the training phase, but these data points are almost limited to the radical line of 10%. Hence, the BPNN model can offer more stable performance and more accurate results.

(a)

(b)

Figure 7. *Cont.*

(**c**)

(**d**)
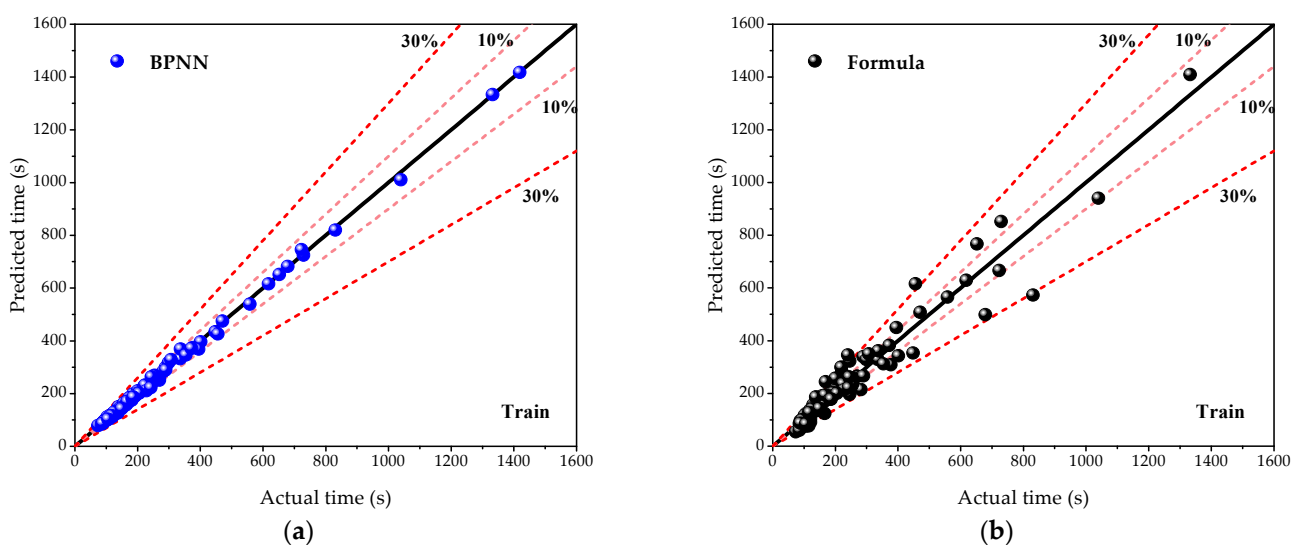
Figure 7. Regression diagrams of both models in the training and testing phase: (**a**) BPNN in training phase; (**b**) empirical formula in training phase; (**c**) BPNN in testing phase; and (**d**) empirical formula in testing phase.

Figure 8 illustrates the error distributions of both models in the training phase and testing phase and some statistical indicators, i.e., the minimum of error ($Error_{min}$), the maximum of error ($Error_{max}$), the mean of error ($Error_{mean}$) and the standard deviation of error ($Error_{St.D}$) are contained in this figure as criteria. The horizontal axes represent the error values between the actual time and the predicted time. The vertical axes are the count within a specified error range. Accordingly, the higher the error bar near the origin and the lower the statistical indicators are, the smaller the model error. As can be realized, the BPNN shows promising results because the region of horizontal axes of the first bar is only from 0 to 10 in the BPNN model when the count of the first bar is almost equal in both models. Additionally, it can be observed that the empirical formula has similar performance in both the training phase and the testing phase.

(**a**)
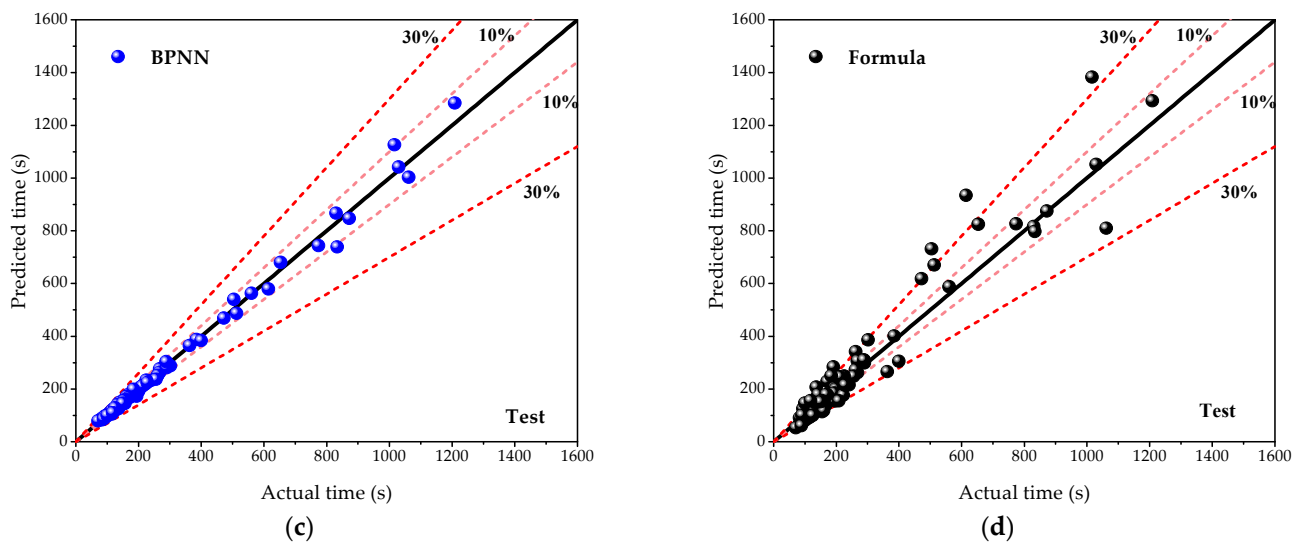

(**b**)
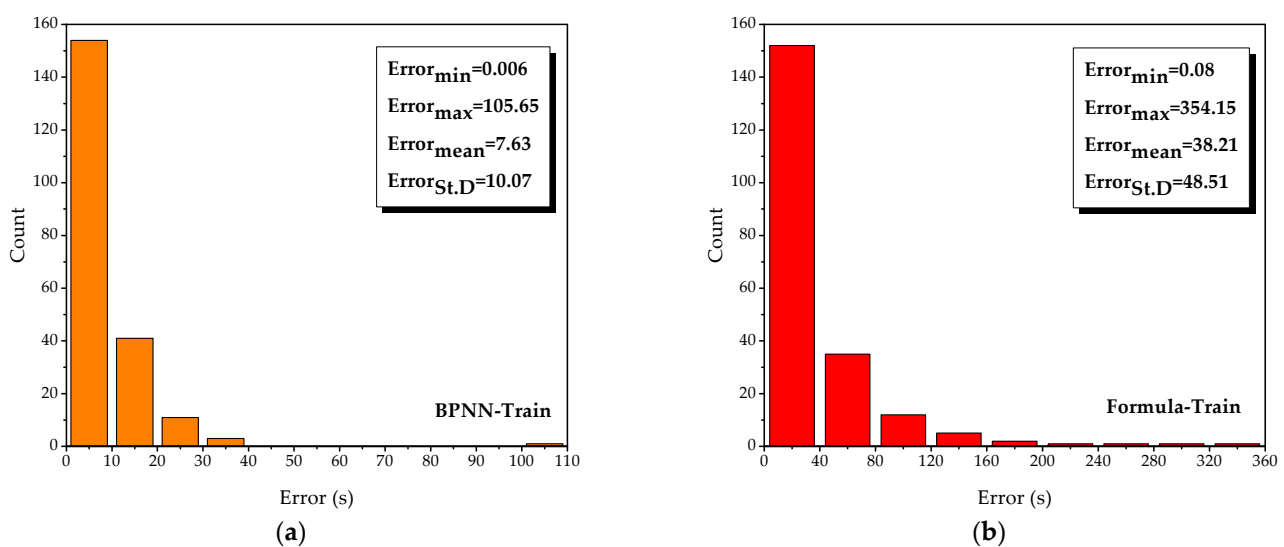
Figure 8. *Cont*.
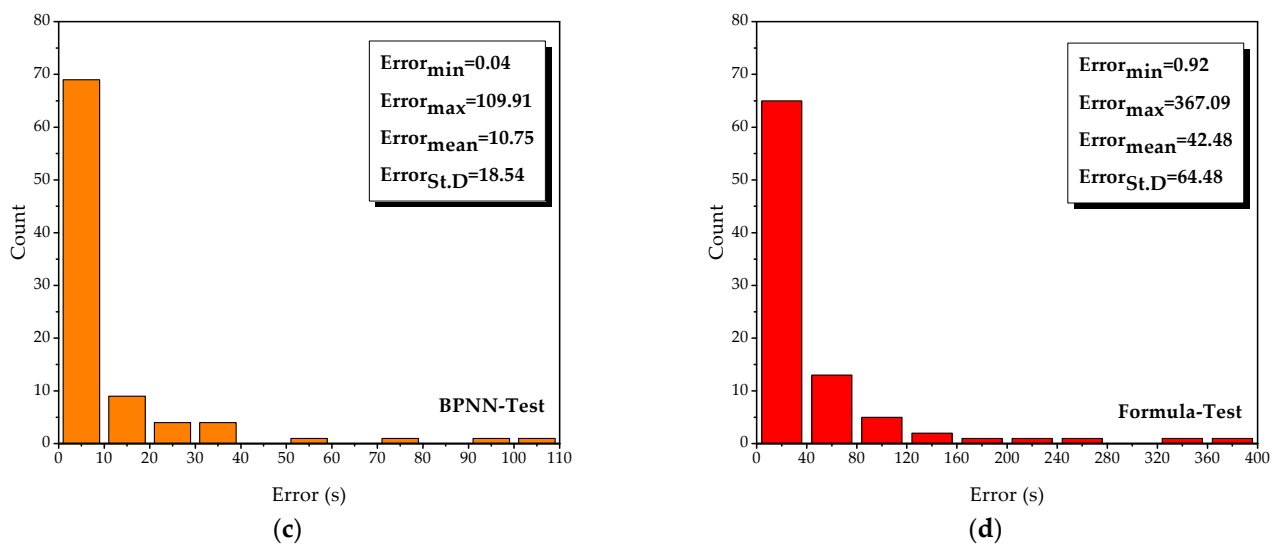
Figure 8. Prediction error comparison of both models in the training and testing phase: (**a**) BPNN in training phase; (**b**) empirical formula in training phase; (**c**) BPNN in testing phase; and (**d**) empirical formula in testing phase.

5. Algorithm Embedding

Given the complicated environment on the site and the inconvenience of running code in the engineering practice, some scientists have performed a lot of work on the application of construction schedule methods, such as the use of software. Song et al. [38] developed a universal engineering construction system simulation software for the construction schedule visualization simulation of hydraulics and hydropower. Wang et al. [10] embedded a ventilation time function in existing software to replace the empirical values for the construction processes and schedule arrangement. In this study, the trained BPNN model was embedded into an existing software module named Simulation Software for Post-blast Re-entry to enhance the performance and facilitate practical use in the central control room located on the surface (see Figure 9). It can be seen that the prediction time obtained from the BPNN model is displayed as both numeric and bar values. Additionally, some optimizations have been applied to the software based on this study. For example, the standard concentration can be input more flexibly according to the requirements rather than using the fixed one. The dilution efficiency factor in the empirical formula was also appended to this software to provide more reference information for users in the period of decision-making. Furthermore, the software can also be utilized to support the formulation of a preliminary schedule. To respond to the call to develop an intelligent mine, interfacing with the mine's integrated system will be the object in future research.
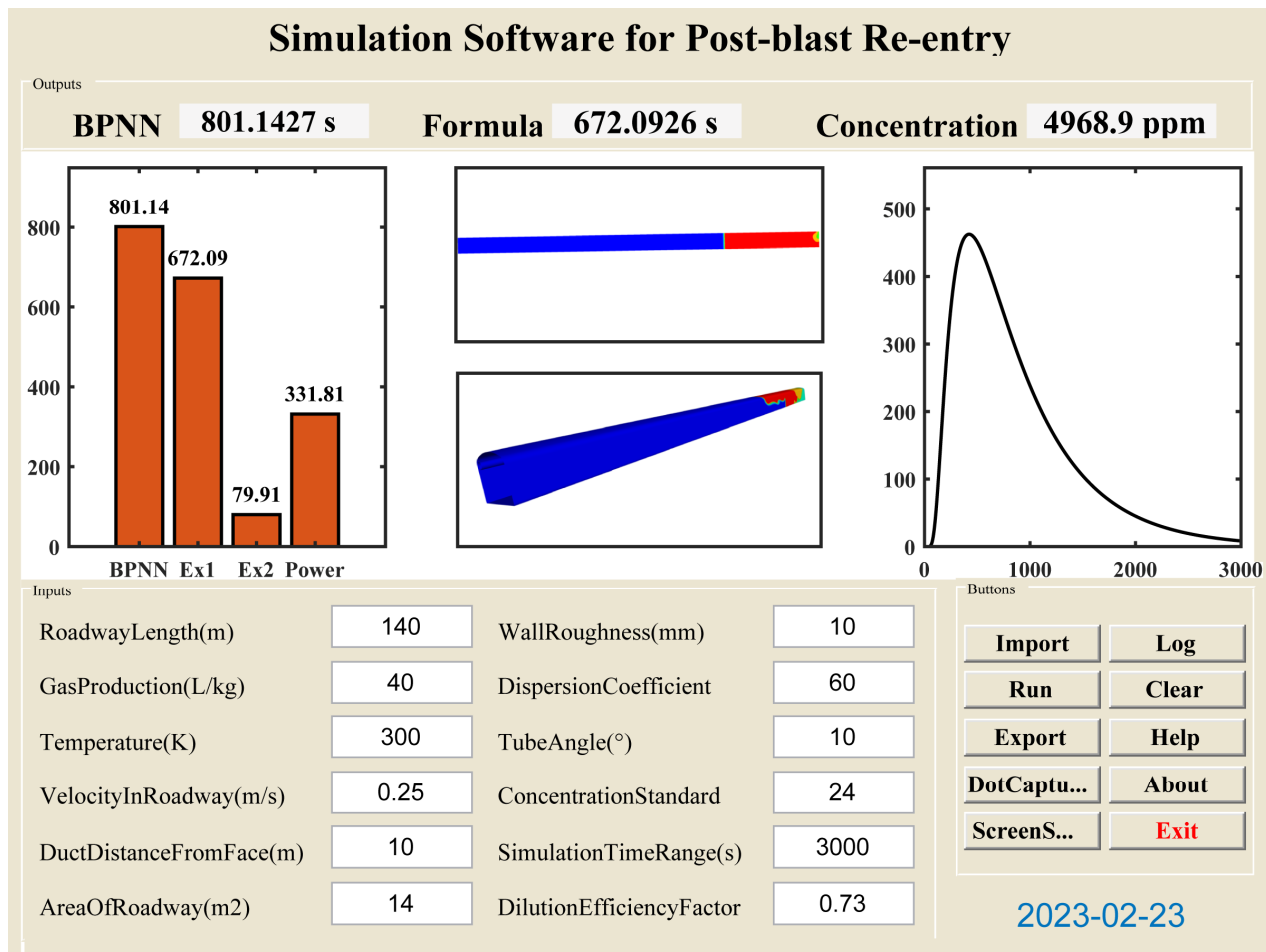
Figure 9. Interface of simulation software for predicting time.

6. Conclusions

Determining the post-blast re-entry time is essential in the excavation field of tunnel and mining to prevent the occurrence of poisoning and asphyxiation incidents. In this paper, a BPNN model was proposed with consideration of four parameters most used in former studies. An empirical formula was calibrated to compare the performance with the proposed BPNN model. It found that the BPNN model with six neurons in the hidden layer outperforms the others. Furthermore, the results show that the BPNN model has a higher reliability and accuracy (RMSE: 21.45; R^2: 0.99; MAE: 10.78; SSE: 40934) compared with the empirical formula (RMSE: 76.89; R^2: 0.90; MAE: 42.06; SSE: 526147). In order to facilitate the engineering use of the BPNN model developed in this study, the model has been embedded in one software application. The operator can not only set schedules for production tasks in advance but also can perform some ventilation optimization by adjusting parameters in this software to facilitate the cleaning efficiency of toxic gases.

This study provides an effective tool for the prediction of post-blast re-entry time in excavation engineering. However, some other influence factors, such as the temperature and the interactions between the wall roughness and the velocity of airflow, etc., may also affect the results; a fact which should be considered to achieve a better agreement between the predicted results and the actual situations. This will be discussed in future research.

Author Contributions: Conceptualization, J.Z. and C.L.; methodology, C.L.; software, J.Z.; validation, J.Z.; formal analysis, J.Z.; investigation, J.Z. and T.Z.; resources, J.Z.; data curation, J.Z.; writing—original draft preparation, J.Z.; writing—review and editing, T.Z. and C.L.; visualization,

J.Z.; supervision, T.Z. and C.L.; project administration, J.Z. All authors have read and agreed to the published version of the manuscript.

Institutional Review Board Statement: Not applicable.

Informed Consent Statement: Not applicable.

Data Availability Statement: See Appendix A.

Conflicts of Interest: The authors declare no conflict of interest.

Appendix A

	Length/(m)	Gas/(L/kg)	Velocity/(m/s)	Limit/(ppm)	Time/(s)
1	469	40.47	1.31	38.52	246
2	921	39.53	2.57	31.90	140
3	1475	40.77	2.33	32.69	185
4	893	37.50	0.38	32.40	1040
5	393	40.27	1.34	24.62	246
6	243	38.16	2.37	37.60	121
7	256	40.40	3.25	33.73	90
8	439	40.02	2.10	41.43	152
9	324	40.61	0.69	29.08	448
10	347	41.58	1.77	44.34	166
11	510	38.91	2.31	31.86	145
12	474	36.20	3.79	33.98	86
13	954	36.09	3.50	38.44	107
14	1145	37.83	1.59	30.45	246
15	1381	36.61	1.99	40.52	201
16	967	39.21	1.72	34.15	221
17	385	41.72	3.21	36.36	94
18	601	38.99	1.03	36.23	336
19	977	36.35	1.92	30.20	200
20	1028	38.84	2.40	38.10	169
21	957	40.69	2.92	41.64	129
22	733	37.23	3.53	25.00	101
23	1459	41.48	3.54	49.79	120
24	307	36.69	0.77	31.24	401
25	363	41.33	0.79	39.60	377
26	535	37.85	3.66	46.26	89
27	1358	37.93	1.17	42.51	337
28	1490	40.42	2.49	34.57	174
29	891	39.11	3.62	35.44	109
30	1388	36.72	3.89	36.69	104
31	1287	38.94	1.65	39.18	270
32	865	41.51	1.08	30.82	354
33	1089	38.02	0.30	27.91	1419
34	271	41.53	0.42	37.10	679
35	799	38.20	3.26	26.70	121
36	1056	40.83	0.92	35.32	456
37	1218	39.50	1.45	24.92	289
38	1261	41.46	2.26	41.85	193
39	540	39.51	3.22	41.22	102
40	1160	36.17	0.55	42.26	729
41	454	41.63	2.36	45.01	131
42	875	39.01	0.47	47.88	723
43	1343	36.12	1.73	26.25	270
44	1414	41.35	1.38	38.31	299
45	606	40.44	3.77	26.08	92

	Length/(m)	Gas/(L/kg)	Velocity/(m/s)	Limit/(ppm)	Time/(s)
46	1002	41.98	1.80	48.54	219
47	1449	37.53	2.19	47.50	193
48	266	39.80	2.53	45.38	115
49	302	41.93	3.31	25.87	95
50	1383	41.23	0.85	45.80	471
51	1033	40.59	1.70	37.31	240
52	1134	38.15	2.47	40.43	157
53	530	41.75	0.88	28.33	395
54	1495	37.79	3.83	28.24	114
55	1302	38.35	2.76	29.16	163
56	779	36.96	2.51	29.41	152
57	931	36.44	1.63	43.76	224
58	487	39.94	1.22	44.68	257
59	246	36.57	1.04	40.81	282
60	322	36.89	3.92	42.72	74
61	1114	36.37	3.69	27.95	120
62	373	39.85	3.13	30.66	98
63	1322	40.91	3.38	37.06	136
64	591	41.14	3.61	29.78	94
65	1363	39.36	2.08	36.44	228
66	467	37.42	1.89	24.50	182
67	771	36.16	1.30	27.20	290
68	317	41.21	2.79	39.35	107
69	738	39.38	1.75	47.09	205
70	809	37.48	1.40	28.99	254
71	916	37.14	1.46	34.98	244
72	1048	41.88	3.02	40.39	138
73	952	39.93	2.24	46.67	167
74	236	38.77	0.34	43.09	831
75	520	36.46	0.61	34.48	558
76	566	36.22	0.94	30.24	372
77	1332	38.68	1.91	44.88	242
78	1221	37.90	0.32	37.69	1332
79	946	37.95	2.94	45.17	126
80	759	40.64	2.03	30.86	183
81	936	38.12	1.19	36.65	307
82	1279	38.09	2.96	43.64	149
83	406	36.83	3.60	45.72	85
84	642	36.32	3.86	44.55	88
85	352	37.98	2.87	27.74	110
86	449	39.46	0.50	25.21	652
87	1211	38.54	3.55	35.19	117
88	1373	37.21	0.64	49.75	618
89	489	37.68	1.69	49.96	187
90	855	37.75	3.56	39.77	106
91	1231	41.73	2.56	47.25	166
92	225	41.01	2.23	27.08	133
93	1292	40.32	1.18	26.87	379
94	446	40.91	1.84	30.32	177
95	804	41.65	0.49	32.07	717
96	1424	38.79	3.72	30.41	111
97	860	38.52	1.52	25.46	250
98	1246	40.86	3.64	25.66	118
99	495	38.49	2.67	35.65	120
100	708	38.59	3.85	32.11	89

	Length/(m)	Gas/(L/kg)	Velocity/(m/s)	Limit/(ppm)	Time/(s)
101	1180	39.75	3.03	49.13	134
102	1038	37.36	1.00	26.04	409
103	576	40.05	3.05	38.77	107
104	1297	36.15	2.32	35.23	194
105	1063	41.38	2.82	26.29	150
106	1068	37.06	3.63	31.65	117
107	814	39.68	1.16	34.36	309
108	794	37.80	2.38	43.72	146
109	1119	38.47	3.45	33.32	111
110	413	37.38	0.68	43.97	463
111	203	41.79	1.15	49.04	242
112	210	40.52	2.59	42.10	109
113	220	39.48	0.86	39.39	331
114	1444	41.80	0.39	24.58	1284
115	748	36.07	2.97	40.02	123
116	1378	39.56	1.78	32.32	269
117	291	36.30	1.82	37.94	164
118	784	39.28	3.78	49.33	91
119	1368	41.60	2.95	29.82	161
120	850	40.00	2.39	44.80	157
121	677	39.98	3.95	38.14	91
122	1282	36.47	3.99	48.92	111
123	934	41.57	2.06	25.12	202
124	703	36.62	1.33	32.90	283
125	690	40.24	3.67	36.56	90
126	1348	39.19	2.90	48.34	135
127	1470	39.83	1.06	27.33	404
128	251	38.96	3.58	28.37	84
129	873	40.39	1.61	42.60	241
130	429	36.25	3.07	28.74	107
131	1226	38.05	1.98	33.57	214
132	261	37.70	2.09	33.15	145
133	545	40.81	1.93	44.59	173
134	698	41.19	0.75	27.54	496
135	1454	39.65	2.63	42.47	161
136	1129	37.65	2.25	37.27	172
137	332	40.72	1.21	31.49	251
138	568	41.50	2.52	42.80	128
139	1124	40.20	1.11	44.38	345
140	926	40.99	3.70	46.63	98
141	880	41.16	2.13	37.73	183
142	1251	36.02	3.17	31.03	136
143	718	37.60	0.81	35.02	430
144	1178	41.13	0.46	43.84	883
145	1241	39.14	0.93	40.18	461
146	444	37.78	3.23	36.48	100
147	1327	37.31	1.27	32.94	363
148	357	39.35	3.52	33.11	87
149	629	40.09	0.82	33.24	404
150	1256	38.44	1.09	46.88	397
151	1434	36.40	1.10	38.93	378
152	682	40.68	2.98	24.08	122
153	657	36.49	2.28	25.25	153
154	652	40.35	0.62	40.60	555
155	1340	38.24	0.99	31.36	468

	Length/(m)	Gas/(L/kg)	Velocity/(m/s)	Limit/(ppm)	Time/(s)
156	1353	40.62	3.48	43.30	113
157	886	36.54	2.48	24.79	159
158	1155	40.74	3.28	47.30	121
159	434	38.86	0.96	46.46	326
160	548	38.39	3.75	25.96	90
161	789	40.37	1.02	48.75	340
162	1170	40.46	2.75	29.28	146
163	992	37.41	2.74	38.98	142
164	688	36.67	1.86	48.96	178
165	1312	37.43	1.79	41.01	254
166	1480	36.52	0.45	31.70	966
167	1150	39.43	1.26	48.29	314
168	378	40.84	0.26	48.50	1113
169	459	37.28	2.71	39.97	116
170	609	39.57	0.76	45.92	417
171	550	36.02	2.61	37.48	129
172	1139	41.68	3.84	39.56	102
173	812	41.28	2.29	47.80	155
174	555	39.16	0.27	32.53	1254
175	710	37.05	0.28	41.56	1213
176	337	36.10	2.02	46.21	147
177	743	41.06	0.95	42.05	381
178	835	40.17	2.69	25.62	137
179	1236	37.04	1.37	45.22	312
180	662	38.10	2.86	30.61	123
181	1216	40.22	3.08	40.64	136
182	1317	39.41	3.81	44.18	120
183	1195	38.81	0.63	26.91	649
184	723	39.88	1.94	28.95	180
185	627	37.26	0.48	36.27	687
186	284	37.57	3.14	41.76	92
187	368	37.09	1.96	38.73	154
188	941	40.30	3.97	32.74	93
189	479	38.32	3.32	47.67	93
190	987	40.10	0.72	35.81	539
191	1462	39.28	0.53	37.40	797
192	342	38.07	0.60	49.38	479
193	286	40.12	3.87	47.05	75
194	1175	37.33	3.46	29.20	116
195	1109	41.28	1.64	28.53	270
196	223	36.39	2.68	32.20	109
197	281	38.67	2.70	33.36	113
198	616	38.30	1.29	43.14	250
199	972	40.89	1.24	24.83	307
200	728	41.56	2.85	37.52	124
201	1404	37.58	2.84	33.94	143
202	1185	41.85	0.98	35.86	414
203	1307	40.49	0.52	46.05	865
204	241	41.11	1.47	45.84	191
205	754	38.25	0.70	39.14	527
206	528	37.13	2.22	33.44	157
207	621	41.95	1.87	34.77	192
208	693	39.09	2.80	43.93	119
209	1023	37.19	2.05	41.06	197
210	901	36.05	0.91	49.17	387

	Length/(m)	Gas/(L/kg)	Velocity/(m/s)	Limit/(ppm)	Time/(s)
211	1015	36.24	1.53	46.96	262
212	1198	37.72	1.07	46.76	385
213	1190	36.84	2.15	27.70	190
214	312	39.60	1.88	40.22	155
215	1409	38.64	0.73	41.26	560
216	1165	39.31	2.34	24.17	171
217	418	39.73	1.49	36.85	214
218	505	36.74	1.14	26.50	290
219	830	38.74	2.21	36.90	166
220	647	38.89	3.39	45.63	101
221	1360	41.05	2.43	28.04	195
222	764	37.35	2.45	48.71	136
223	388	38.02	3.68	42.68	83
224	1073	39.04	0.83	29.62	513
225	464	39.26	1.55	41.47	205
226	304	39.05	1.35	48.84	217
227	1200	40.02	1.54	32.28	268
228	1393	39.06	3.09	25.41	157
229	825	36.77	3.40	37.89	107
230	1058	39.90	1.39	42.89	302
231	1485	38.17	1.62	46.42	268
232	649	37.94	1.76	39.48	195
233	769	39.78	0.40	41.68	830
234	1271	39.95	0.57	29.57	774
235	713	41.36	3.15	46.84	110
236	1421	40.16	3.44	48.00	120
237	327	39.23	2.99	35.40	100
238	962	36.94	0.58	28.78	653
239	853	39.79	3.29	38.64	115
240	383	36.59	2.78	47.71	108
241	1053	37.56	0.71	47.92	504
242	296	38.62	0.80	24.37	400
243	581	37.73	0.41	26.45	872
244	586	39.70	2.44	24.42	150
245	974	38.61	2.83	49.88	135
246	911	41.70	0.29	43.55	1209
247	820	41.83	3.74	40.85	96
248	525	38.00	1.32	34.40	261
249	870	36.81	3.01	34.19	128
250	1094	41.78	2.16	31.28	201
251	896	40.57	3.18	27.29	125
252	423	41.04	3.51	34.82	92
253	1007	36.68	0.84	43.51	472
254	365	39.13	2.60	26.16	121
255	398	37.88	0.87	29.99	363
256	1013	39.33	2.93	28.16	136
257	1104	39.63	0.37	34.61	1016
258	1137	37.28	3.37	27.00	135
259	632	38.69	1.85	28.12	198
260	1266	37.63	3.43	24.21	127
261	637	40.94	2.72	49.58	123
262	1299	41.94	3.90	34.28	115
263	611	37.46	3.33	31.45	105
264	774	40.79	1.57	35.61	241
265	1419	37.11	2.55	25.04	194

	Length/(m)	Gas/(L/kg)	Velocity/(m/s)	Limit/(ppm)	Time/(s)
266	1035	39.72	2.14	31.16	191
267	1398	40.07	1.90	28.58	256
268	982	38.72	3.35	41.89	115
269	276	36.99	1.56	25.83	197
270	845	38.46	1.68	39.68	222
271	205	38.42	1.42	29.37	208
272	500	41.43	3.93	27.49	83
273	1338	40.67	0.56	38.56	834
274	731	38.83	3.06	30.12	116
275	561	40.54	1.41	45.59	225
276	667	41.41	1.67	33.78	212
277	1205	36.27	2.41	42.93	172
278	484	40.15	0.33	30.03	1030
279	906	38.40	2.17	44.13	162
280	215	37.51	3.76	36.02	71
281	1096	38.91	3.98	40.72	94
282	1079	40.25	2.00	49.54	184
283	840	36.42	0.35	44.97	1062
284	1018	41.09	0.65	33.53	614
285	515	41.31	3.41	43.34	91
286	1084	36.64	3.10	36.06	139
287	1099	36.79	2.64	46.01	142
288	1464	37.01	3.30	44.76	129
289	672	36.91	1.23	47.46	290
290	1277	41.26	2.62	31.07	168
291	403	38.22	2.01	27.12	160
292	1439	38.37	3.16	38.35	133
293	571	38.57	2.11	48.09	154
294	1259	36.91	2.91	35.52	150
295	408	41.90	2.46	32.49	125
296	230	37.16	3.20	48.13	89
297	997	39.58	3.91	26.66	100
298	1043	38.27	3.49	45.42	118
299	1429	40.96	1.44	39.81	288
300	596	36.86	1.50	42.30	228

References

1. Cigla, M.; Yagiz, S.; Ozdemir, L. Application of tunnel boring machines in underground mine development. In Proceedings of the International Mining Congress and Exhibition, Turkey, Ankara, 19–22 June 2001.
2. Zheng, Y.L.; Zhang, Q.B.; Zhao, J. Challenges and opportunities of using tunnel boring machines in mining. *Tunn. Undergr. Space Technol.* **2016**, *57*, 287–299. [CrossRef]
3. Pu, Q.; Luo, Y.; Huang, J.; Zhu, Y.; Hu, S.; Pei, C.; Zhang, G.; Li, X. Simulation study on the effect of forced ventilation in tunnel under single-head drilling and blasting. *Shock. Vib.* **2020**, *2020*, 8857947. [CrossRef]
4. Bahrami, D.; Yuan, L.; Rowland, J.H.; Zhou, L.; Thomas, R. Evaluation of post-blast re-entry times based on gas monitoring of return air. *Min. Metall. Explor.* **2019**, *36*, 513–521. [CrossRef]
5. Menéndez, J.; Merlé, N.; Fernández-Oro, J.M.; Galdo, M.; de Prado, L.Á.; Loredo, J.; Bernardo-Sánchez, A. Concentration, propagation and dilution of toxic gases in underground excavations under different ventilation modes. *Int. J. Environ. Res. Public Health* **2022**, *19*, 7092. [CrossRef]
6. Chen, J.; Qiu, W.; Rai, P.; Ai, X. Emission characteristics of CO and NOx from tunnel blast design models: A comparative study. *Pol. J. Environ. Stud.* **2021**, *30*, 5503–5517. [CrossRef]
7. Gillies, A.D.S.; Wu, H.W.; Shires, D. Development of an assessment tool to minimize safe after blast re-entry time to improve the mining cycle. In Proceedings of the Tenth US/North American Mine Ventilation Symposium, Anchorage, AK, USA, 16–19 May 2004.
8. De Souza, E. Procedures for mitigating safety risks associated with post-blast re-entry times. *CIM J.* **2023**, *14*, 2–10. [CrossRef]
9. Torno, S.; Torano, J.; Ulecia, M.; Allende, C. Conventional and numerical models of blasting gas behaviour in auxiliary ventilation of mining headings. *Tunn. Undergr. Space Technol.* **2013**, *34*, 73–81. [CrossRef]
10. Wang, X.L.; Liu, X.P.; Sun, Y.F.; An, J.; Zhang, J.; Chen, H.C. Construction schedule simulation of a diversion tunnel based on the optimized ventilation time. *J. Hazard. Mater.* **2009**, *165*, 933–943. [CrossRef]

11. Souza, E.D.; Katsabanis, P.D. On the prediction of blasting toxic fumes and dilution ventilation. *Eng. Geol.* **1991**, *13*, 223–235. [CrossRef]
12. Hebda-Sobkowicz, J.; Gola, S.; Zimroz, R.; Wylomanska, A. Identification and statistical analysis of impulse-like patterns of carbon monoxide variation in deep underground mines associated with the blasting procedure. *Sensors* **2019**, *19*, 2757. [CrossRef]
13. Torno, S.; Toraño, J. On the prediction of toxic fumes from underground blasting operations and dilution ventilation. Conventional and numerical models. *Tunn. Undergr. Space Technol.* **2020**, *96*, 103194. [CrossRef]
14. Zhou, Y.; Yang, Y.; Bu, R.W.; Ma, F.; Shen, Y.J. Effect of press-in ventilation technology on pollutant transport in a railway tunnel under construction. *J. Clean. Prod.* **2020**, *243*, 118590. [CrossRef]
15. Stewart, C.M. Practical prediction of blast fume clearance and workplace re-entry times in development headings. In Proceedings of the 10th International Mine Ventilation Congress, Sun City, South Africa, 2–8 August 2014.
16. Li, C.Q.; Zhou, J.; Armaghani, D.J.; Cao, W.Z.; Yagiz, S. Stochastic assessment of hard rock pillar stability based on the geological strength index system. *Geomech. Geophys. Geo-Energy Geo-Resour.* **2021**, *7*, 47. [CrossRef]
17. Li, J.; Li, C.; Zhang, S. Application of six metaheuristic optimization algorithms and random forest in the uniaxial compressive strength of rock prediction. *Appl. Soft Comput.* **2022**, *131*, 109729. [CrossRef]
18. Li, C.; Zhou, J.; Dias, D.; Gui, Y. A kernel extreme learning machine-grey wolf optimizer (KELM-GWO) model to predict uniaxial compressive strength of rock. *Appl. Sci.* **2022**, *12*, 8468. [CrossRef]
19. Zhou, J.; Li, E.; Wei, H.; Li, C.; Qiao, Q.; Armaghani, D.J. Random forests and cubist algorithms for predicting shear strengths of rockfill materials. *Appl. Sci.* **2019**, *9*, 1621. [CrossRef]
20. Li, C.; Zhou, J.; Khandelwal, M.; Zhang, X.; Monjezi, M.; Qiu, Y. Six novel hybrid extreme learning machine–swarm intelligence optimization (ELM–SIO) models for predicting backbreak in open-pit blasting. *Nat. Resour. Res.* **2022**, *31*, 3017–3039. [CrossRef]
21. Eslami, E.; Choi, Y.; Lops, Y.; Sayeed, A. A real-time hourly ozone prediction system using deep convolutional neural network. *Neural Comput. Appl.* **2019**, *32*, 8783–8797. [CrossRef]
22. Wang, Y.; Liu, P.; Xu, C.; Peng, C.; Wu, J. A deep learning approach to real-time CO concentration prediction at signalized intersection. *Atmos. Pollut. Res.* **2020**, *11*, 1370–1378. [CrossRef]
23. Li, C.Q.; Zhou, J.; Armaghani, D.J.; Li, X.B. Stability analysis of underground mine hard rock pillars via combination of finite difference methods, neural networks, and Monte Carlo simulation techniques. *Undergr. Space* **2021**, *6*, 379–395. [CrossRef]
24. Huang, R.Y.; Shen, X.; Wang, B.; Liao, X. Migration characteristics of CO under forced ventilation after excavation roadway blasting: A case study in a plateau mine. *J. Clean. Prod.* **2020**, *267*, 122094. [CrossRef]
25. Chang, P.; Xu, G.; Zhou, F.; Mullins, B.J.; Abishek, S.; Chalmers, D. Minimizing DPM pollution in an underground mine by optimizing auxiliary ventilation systems using CFD. *Tunn. Undergr. Space Technol.* **2019**, *87*, 112–121. [CrossRef]
26. Toraño, J.; Torno, S.; Menéndez, M.; Gent, M.R.; Velasco, J. Models of methane behaviour in auxiliary ventilation of underground coal mining. *Int. J. Coal Geol.* **2009**, *80*, 35–43. [CrossRef]
27. Wei, N.; Zhong-an, J.; Dong-mei, T. Numerical simulation of the factors influencing dust in drilling tunnels: Its application. *Min. Sci. Technol. (China)* **2011**, *21*, 11–15. [CrossRef]
28. Zhang, H.; Sun, J.; Lin, F.; Chen, S.; Yang, J. Optimization scheme for construction ventilation in large-scale underground oil storage caverns. *Appl. Sci.* **2018**, *8*, 1952. [CrossRef]
29. Bismark, A.; Opafunso, Z.O.; Oniyide, G.O. Predicting the re-entry time at Chirano Gold Mine limited southwestern Ghana using ventsim simulation software. *Niger. J. Eng.* **2022**, *29*, 102–112.
30. GB 16423-2020*Safety Regulation for Metal and Nonmetal Mines*; Ministry of Emergency Management of the People's Republic of China: Beijing, China; Emergency Management Press: Beijing, China, 2020.
31. AQ 2031-2011*Regulations for The Construction of Monitoring and Supervision System in Metal and Nonmetal Underground Mine*; Ministry of Emergency Management of the People's Republic of China: Beijing, China; China Coal Industry Publishing House: Beijing, China, 2011.
32. Zawadzka-Małota, I. Testing of mining explosives with regard to the content of carbon oxides and nitrogen oxides in their detonation products. *J. Sustain. Min.* **2015**, *14*, 173–178. [CrossRef]
33. Brake, D.J. A review of good practice standards and re-entry procedures after blasting and gas detection generally in underground hardrock mines. In Proceedings of the 15th North American Mine Ventilation Symposium, Blacksburg, VA, USA, 21–23 June 2015; pp. 20–25.
34. Wang, Y.M. *Mine Ventilation and Dust Control*; Metallurgical Industry Press: Beijing, China, 1993; p. 198.
35. Wang, X.G. *Emulsion Explosives*, 2nd ed.; Metallurgical Industry Press: Beijing, China, 2008; p. 575.
36. Zhao, H.; Wang, Y.J.; Song, J.; Gao, G. The pollutant concentration prediction model of NNP-BPNN based on the INI algorithm, AW method and neighbor-PCA. *J. Ambient. Intell. Hum. Comput.* **2018**, *10*, 3059–3065. [CrossRef]
37. Zhang, J.; Dias, D.; An, L.; Li, C. Applying a novel slime mould algorithm-based artificial neural network to predict the settlement of a single footing on a soft soil reinforced by rigid inclusions. *Mech. Adv. Mater. Struct.* **2022**, 1–16. [CrossRef]
38. Song, Y.; Zhong, D.H. Study on construction schedule management and control method for hydraulic & hydropower engineering based on visual simulation. *Syst. Eng.-Theory Pract.* **2006**, *8*, 55–62. [CrossRef]